7th International Conference on Innovation in High Performance Sailing Yachts and Wind-Assisted Ships. InnovSail 2026, Gothenburg, Sweden, 3-5 June 2026.

VPP-Driven Sail and Foil Trim Optimization for the Olympic NACRA 17 Foiling Catamaran

K. Graf
University of Applied Sciences Kiel (retired professor), Germany, kai.graf@sailingvpp.com

Abstract. The Nacra-17 is the current Olympic catamaran sailed in the Olympic Games since 2016 by a mixed crew. Over the years, the boat has undergone some changes. The initial design of the boat featured a set of appendages that only rarely allowed the boat to foil. Today, Nacra-17 features semi-L-shaped daggerboards and T-rudders, all of them independently trimmable. This allows the boat to foil at wind speeds of 9 kts and below on an upwind tack and even earlier on a downwind tack. Trimming flexibility comes at the cost of increased complexity in sailing the boat. This project addresses this challenge by assisting sailors in identifying an optimized set of trim parameters using a proprietary velocity prediction program, which—beyond solving the equilibrium of all forces acting on the boat—searches for a combination of daggerboard and rudder rake, rudder angle, heel angle, and platform trim that maximizes performance. The method and selected results are also discussed.

Keywords: sailing; Nacra-17; VPP; foils; optimization

NOMENCLATURE

Variables:

AD	Drag area [m²]
AD_0	*AD* at zero *LW* and *pitch* [m²]
AL	Lift Area [m²]
AL_0	Lift area at zero *LW* and *pitch* *[m²]*
A_{Ref}	Reference sail area [m²]
AS	Spanwise force area [m²]
AS_0	*AS* at zero *LW* and *pitch* *[m²]*
AWA	Apparent wind angle [°]
AWS	Apparent wind speed [m s^{-1}]
c_D	Drag coefficient [-]
c_{D0}	Drag coefficient at zero lift [-]
$c_{D\ sailed}$	Drag coefficient of depowered sail [-]
CE	Efficiency coefficient [-]
c_L	Lift coefficient [-]
$c_{L\ DOWN}$	Downwind sail set lift coefficient [-]
$c_{L\ sailed}$	Lift coefficient of depowered sail [-]
$c_{L\ UP}$	Upwind sail set lift coefficient [-]
c_S	Spanwise force coefficient [-]
d_f	Daggerboard response surface coefficient [-]
d_U	Daggerboard response surface coefficient [-]
E	Main sail foot length [m]
$EMAR$	Effective main sail aspect ratio [-]
F_L	Aerodynamic lift force [N]
fly	Height of origin above water plane [mm]
$flat$	Sail depowering factor [-]

I Distance deck to forestay hounds [m]
J Distance foresail tack to mast [m]
kpp Sail parasitic profile drag coefficient [-]
L Daggerboard lift [N]
l_f Daggerboard response surface coefficient [-]
l_U Daggerboard response surface coefficient [-]
LW Leeway angle [°]
m_D Moment coefficient around D-axis [°]
m_L Moment coefficient around L-axis [°]
m_S Moment coefficient around S-axis [°]
P Main sail luff length [m]
pitch,rake Daggerboard rotation around transverse axis [°]
RA Rudder angle [°]
s_f Daggerboard response surface coefficient [-]
s_U Daggerboard response surface coefficient [-]
TWA True wind angle [°]
TWS True wind speed [m s^{-1}]
U, speed Boat speed [m s^{-1}]
VMG Velocity made good [m s^{-1}]
ϕ, *heel* Platform heeling angle [°]
ρ Density of water [1000 kg m^{-3}]
ρ_{Air} Density of air [1.25 kg m^{-3}]

Acronyms:
BRICS blended reconstructed interface capturing scheme
CFD Computational Fluid Dynamics
DLS Drag-lift-span coordinate system
ORC Offshore Racing Council, this abbreviation is widely used for the ORC measurement system
VMG Velocity Made Good
VPP Velocity Prediction Program
XYZ boat longitudinal, transverse, upright coordinate system

1 INTRODUCTION

The Nacra-17 catamaran, sailed by a mixed crew, has served as the Olympic multihull class since the 2016 Olympic Games. Since then, designers have modified daggerboards and rudders multiple times. For the Olympic Games 2020(21), the previously used C-shaped daggerboards were replaced by semi-L-shaped ones, which, together with T-rudders, allow the catamaran to fly. After the 2021 Olympic Games, another change was made. The rudder rake, formerly fixed for a race duration, is now adjustable while racing.

Although these design changes have transformed Nacra-17 into a highly attractive catamaran capable of delivering spectacular racing, they have made the boat very complex to sail. A Nacra-17 crew faces numerous challenges in sailing boats competitively. While the boat is physically demanding and proper boat handling is the key to success on the race-course, the Nacra-17 also provides some technical and tactical challenges unknown in other boat-classes. Proper trim of rudders and daggerboards is crucial for the best performance. Under light wind conditions, crews may achieve maximum VMG either by foiling or by non-foiling; although both approaches can yield the same maximum VMG, they differ substantially in tactical execution.

Consequently, training in this class involves a continuous search for the optimal trim of the rig and sails as well as the hydrodynamic elements, particularly the daggerboard and rudder settings. Proper daggerboard and rudder trim not only rely on the onset of foiling but also on foiling and non-foiling performance as well as manageability in rough and unsteady conditions. Training aims not only to improve boat-handling skills but also to build experience in optimal trim selection and effective use of all aerodynamic and hydrodynamic trimming options. This article presents an accompanying theoretical study that assists the crew in identifying the optimal overall trim for the Nacra-17, including aerodynamic and hydrodynamic elements.

Figure 1. Nacra-17 foiling (Source: Kohlhoff/Stuhlemmer Sailing Team)

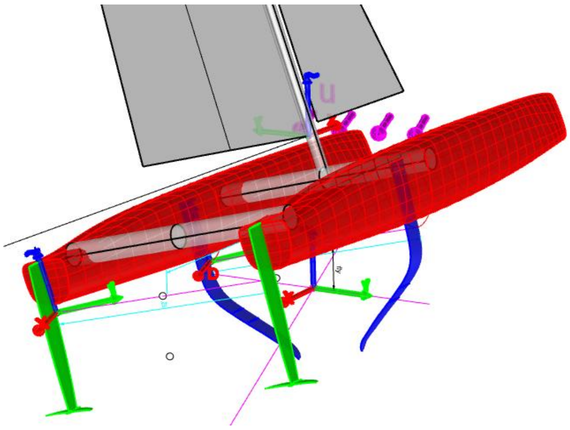

Figure 2. Semi-L daggerboards and T-rudders of the Nacra-17 (conceptual model)

Table 1. Nacra-17 main dimensions

Length:	5.25 m
Beam:	2.59 m
Weight empty:	138 kg
Sail Area:	
Upwind:	20.1 m²
Downwind:	39.6 m²
Designer:	Morrelli & Melvin

To achieve this aim, the study develops a dedicated velocity prediction program (VPP) to determine optimal trim settings for boat aerodynamic and hydrodynamic components. The VPP estimates boat speed by calculating force and moment equilibrium in four degrees of freedom, while non-equality constraints are considered for the remaining two degrees of freedom, namely the total heeling and pitching moment. The optimal combination of sail and foil trim parameters is found using a nonlinear constrained optimization method. Flow forces are predicted using various flow analysis methods: sail forces are taken from wind tunnel test results with a 1:5.6-scale model of the Nacra-17. Hull, daggerboard and rudder forces and moments are derived from free-surface RANS flow simulations, which execute a large simulation test matrix, considering a range of fly-, leeway-, pitch- and heel-states, as well as velocities.

The following chapters describe the flow-force prediction methods and the optimization procedure before presenting the results.

2 STATE OF THE ART AND BIBLIOGRAPHY

Any sailing boat VPP relies on methods that predict all flow forces acting on the boat. This project uses wind tunnel tests to determine aerodynamic forces and free-surface RANS simulations to predict hull and daggerboard hydrodynamic forces.

Wind tunnel tests were conducted at the twist flow wind tunnel of the University of Applied Sciences Kiel, utilizing a 1:5.6 scale model of the Nacra-17. A general description of the wind tunnel test procedure for sails is given by Clauthon et al. (1998). Aerodynamic lift and drag prediction follow *Hazen's* (1980) principles. A quite modern variant of Hazen's approach is used by the ORC measurement system, Offshore Racing Congress (2024). However, the Nacra-17 rig shows some features not comparable with a modern cruiser/racer rig as addressed by the ORC system: the jib and the gennaker are quite small and the jib foot does not reach a deck. The main sail headboard is very large, and twist of the main sail is a key component of fast sailing. Since these features are only poorly modeled by the standard Hazen method, a proprietary extension is developed and used in the Nacra-17 VPP. This is described in section 4.3 and 4.4.

More advanced aerodynamic flow prediction methods were developed by Knudsen et al. (2023), trying to model the structural behavior of the rig and the sails of the Nacra-17 in a fluid–structure interaction method together with RANS-based sail force prediction. No attempt is made here to follow their approach for the simple reason of computational costs.

A proprietary solution method based on the OpenFOAM framework was used for free-surface RANS simulations of flow around hull, daggerboard and rudder. The standard free-surface-flow method within the OpenFOAM framework, *interFoam*, uses very small time-steps for the transient RANS-simulation and still suffers from numerical diffusion of the free surface. Our proprietary free-surface solver, based on OpenFOAM, implements advanced differencing schemes for fractional volume-of-fluid advection, similar to those used in the ISIS solver described by Wackers et al. (2011). Our RANS-solver is described in Meyer et al. (2016), and its validation and application to fast sailing yacht flow problems are described in Graf et al. (2017).

The general solution method for velocity prediction is based on constrained optimization. An interior-point method is used, which predicts Jacobians with forward differencing and the Hessian from the iterative history of Jacobian calculation; see Nocedal and Wright (2016). No effort has been made to implement or adapt a proprietary solution method for the particular purpose of this project. Instead, Matlab™ is used as the numerical computation framework.

This article is a follow-up of a presentation published at a previous *InnovSail* conference, Graf and Freiheit (2020). The article describes new methods, achievements and results, obtained in the years 2021–2024, the latest Olympic cycle. Some of the methods from the 2020 publication are briefly outlined as far as they serve the understanding. Some new results contradict earlier findings, and this paper explains the reasons for these discrepancies.

3 COORDINATE SYSTEM

Various coordinate systems are used, see Figure 3. The boat is sailing on a course with wind from the starboard. The drag-lift-span (DLS) coordinate system is a local coordinate system used for the daggerboard, rudder and sails. The DLS axes are oriented in the flow direction, perpendicular to flow and span, and in the spanwise direction. For L-shaped or semi-L-shaped daggerboards and for the T-rudders, the definition of spanwise force is arbitrary, since spanwise force is a lift as well. In this case, the span direction at the foil root is used as a spanwise direction. Since the drag axes D is aligned with the incident flow, being different for daggerboard and rudder as well as the sails, the DLS-axis is a local one, differing for any foil and the sails. Drag, lift and spanwise force are calculated in these local coordinate systems.

The origin of these local coordinate systems is set to:

- The intersection of the leading edge with the hull for the daggerboard.
- The intersection of the rudder leading edge with a virtual smooth hull extension for the rudder.
- The gooseneck projected to the water surface for the sail set.

Flow forces in the DSL-coordinate system are first transferred to the x',y',z' coordinate system, a coordinate system fixed to the centerline of the boat (x') and the mast (z'). The model assumes that the crew-induced righting moment acts about the x'-axis; accordingly, the heeling-moment constraint is defined in this coordinate system. Flow forces are then transferred to the XYZ-coordinate system. The X-axis of the XYZ-coordinate system points in the direction of the undisturbed hydrodynamic incident flow, the Z-axis points perpendicular to the undisturbed water surface. The equilibrium of flow forces is established in this latter coordinate system.

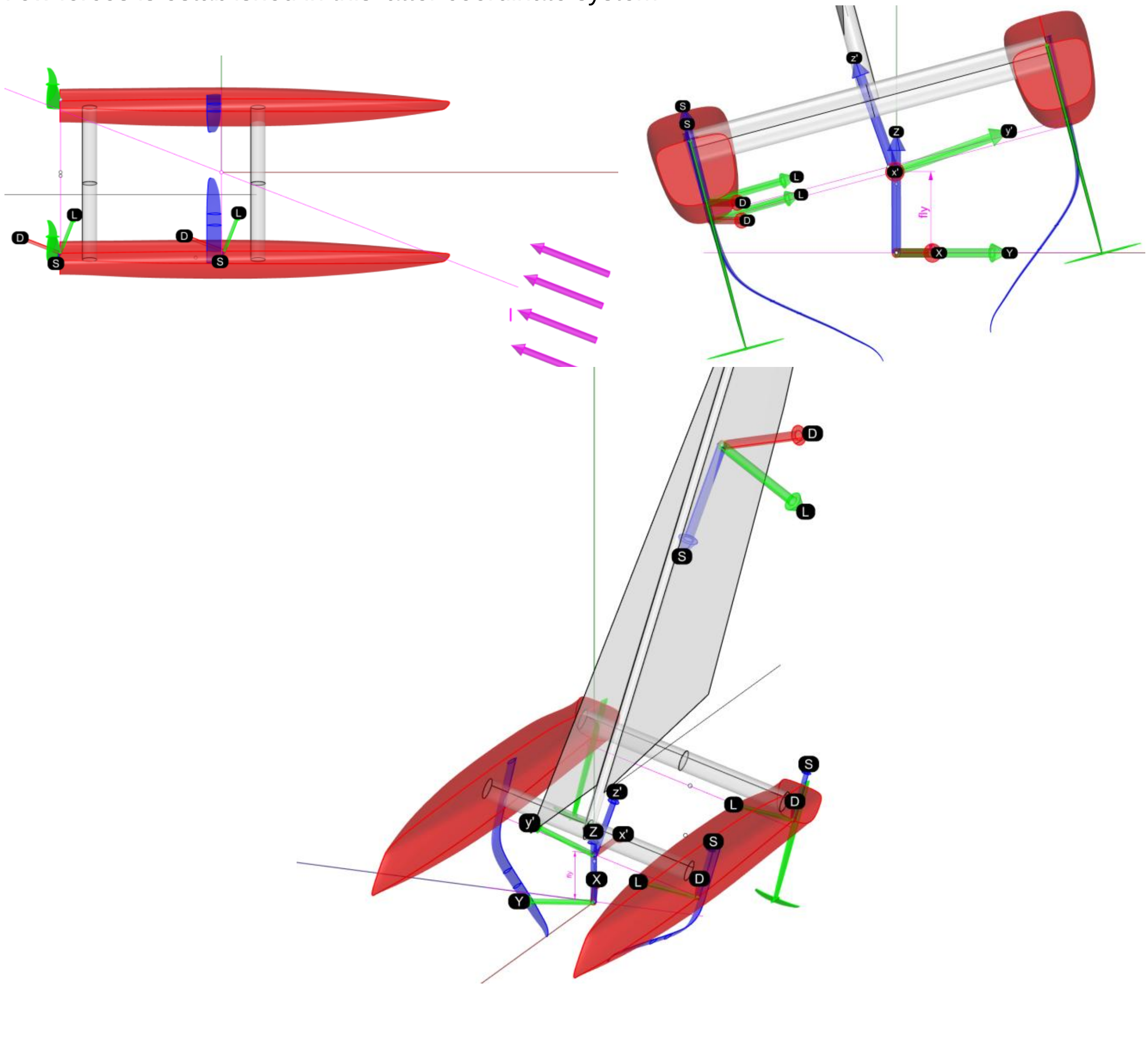

Figure 3. Coordinate systems

4 AERODYNAMIC FLOW FORCES

The aerodynamic flow forces of the Nacra-17 were investigated in the wind tunnel of our university. The wind tunnel is an open, constant-pressure type tunnel, generating twisted flow, mimicking the height-dependent apparent wind a sailing yacht encounters while sailing. The wind tunnel is equipped with a high precision 6-DOF force balance and laser-Doppler anemometry for wind speed measurements.

A Nacra-17 model with a scale factor of 1:5.6 was built. While the rig is modeled quite accurately, the hull shape is only approximated, and a box equipped with servo motors was placed between the hulls to host the trim actuators. Measurement results were obtained by trimming the sails manually for maximum driving force in an upright position (no heel).

Servo motors allowed trimming mainsail sheet, boom vang, mast rotation, jib sheet and jib barberhaul. On downwind tack tests the servos trimmed the gennaker sheet and the gennaker tack line. The sails were made from Mylar film and fitted with stiffeners to create a curved profile. They can be regarded as stiff. They buckled under the force of the wind, yet the canvas did not stretch.
Tests were conducted for the upwind case with a mainsail and a jib and for the downwind case, in which an additional gennaker was used. Two simplified dummy bodies account for the drag of the crew in trapeze conditions.

An aerodynamic model processes raw wind tunnel force data to account for sail trimming by the crew, particularly sail flattening, traveler easing, and the introduction of sail twist.

Figure 4. Nacra-17 model, scale 1:5.6 in the twist flow wind tunnel

4.1 Standard Hazen Aerodynamic Model

The first implementation of the Nacra-17 VPP as to Graf and Freiheit (2020) used an aerodynamic force model based on the work of Hazen (1980) and the more modern incarnation of Hazens method used by the ORC, Offshore Racing Congress (2024). This force model is quite accurate for 3-DOF VPPs as the ORC VPP; however, for a 6-DOF-VPP of a foiling catamaran, it turned out to be insufficient for a couple of reasons:

- Only lift and drag coefficients are used to calculate respective forces. Heeling moments are calculated with a single constant center of effort height of the side and driving force. No method is given to predict yawing and pitching moments. Vertical forces are ignored.
- The drag coefficient, c_D, is calculated from the drag coefficient at zero lift c_{D0}, and the induced drag, predicted with the lift coefficient c_L squared and an efficiency coefficient, CE:

$$c_D = c_{D0} + CE \cdot c_L^2 \quad (1)$$

where *CE* incorporates the parasitic profile drag coefficient *kpp* and the effective span *EMAR* of the rig to calculate the induced drag:

$$CE = kpp + \frac{1}{\pi \, EMAR} \tag{2}$$

EMAR is computed from the geometric data of the rig by some regression formulas. It does not consider specific details of the Nacra-17, in particular, the very large headboard and the jib foot not reaching the deck. In addition, the jib is quite small compared to the main sail, which is not found in typical ORC-yachts.

- The twist of the main sail is only considered a correction of sail flattening: twisting the sail is always bound to lift reduction due to reduced profile depth or traveler easing.
- The standard Hazen model features a *reef* coefficient, describing a reduction of the luff of the sails. Since the Nacra-17 is never reefed, this reef coefficient is obsolete.

The above approach may be accurate for rigs following the standard ratios of principle dimensions for an ORC-type yacht, but its accuracy for rigs that deviate from standard dimensions is limited.

Here, a new approach to sail force calculation is implemented. It is based on three principles:

- 6-DOF coefficient sets are used.
- Induced drag is computed with an effective span, which is derived from measurements rather than from rig geometry.
- An independent twist variable is introduced, which reduces the heeling moment as well as the effective span of the sail, thus increasing induced drag.

4.2 6-DOF Sail Coefficients

For our current VPP, a variation of the standard Hazen approach is used. Aerodynamic forces and moments are measured in six DOF. Consequently, six coefficients can be predicted from the measurements: drag-, lift- and spanwise force coefficients c_L, c_{D0} and c_S as well as respective moment coefficients m_D, m_L and m_S are defined as follows:

$$c_{L,D,S} = \frac{F_{L,D,S}}{0.5 \rho \, AWS^2 \, A_{Ref}} \tag{3}$$

$$m_{L,D,S} = \frac{M_{L,D,S}}{0.5 \rho \, AWS^2 \, A_{Ref}^{1.5}} \tag{4}$$

The reference area A_{Ref} is calculated from the rig dimensions:

$$A_{Ref} = 0.5(E\,P + I\,J) \tag{5}$$

Figure 5 and Figure 6 show lift and drag coefficients as well as moment coefficients measured in the twist flow wind tunnel. Because sail trimming is performed manually, the results contain noise and require smoothing using the least-squares method.

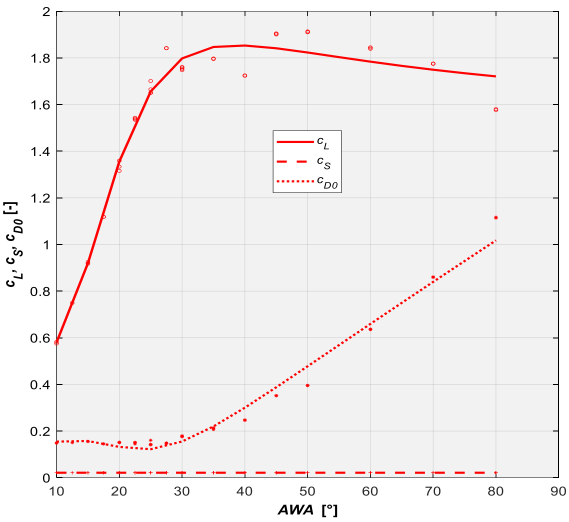

Figure 5. Lift and drag coefficient of Nacra-17 rig

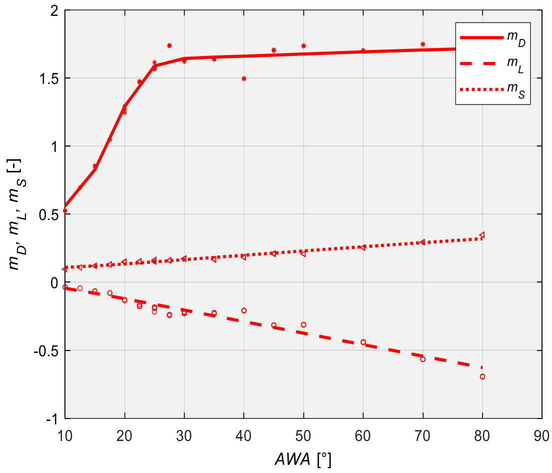

Figure 6. Moment coefficients Nacra-17

The spanwise forces measured in the wind tunnel are about two orders of magnitude smaller than the measured lift forces. Therefore, these values are not trusted and are set to a single averaged value.

4.3 Effective Span

For apparent wind angles (AWA) in the range $10° \leq AWA \leq 25°$, the sail follows almost linear wing theory, which means $\partial c_L / \partial AWA$ is a constant. In this linear regime, the drag coefficient depends linearly on the lift coefficient squared, see Figure 7.

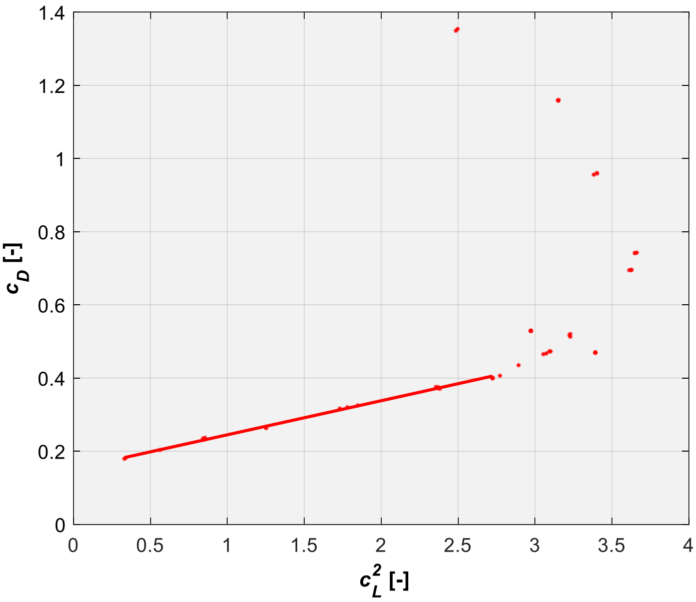

Figure 7. Drag coefficient over lift coefficient squared

From the graph slope (Figure 7), the effective span S_E of the rig can be computed as follows:

$$S_E = \sqrt{\frac{A_{Ref}}{\pi \ \ \partial c_D / \partial(c_L^2)}} \tag{6}$$

S_E in turn can be used to compute an efficiency coefficient of the induced drag:

$$CE = \frac{c_{Di}}{c_L^2} = \frac{A_{Ref}}{S_E^2\,\pi} \tag{7}$$

For simplification, in these expressions, the parasitic profile drag is treated together with the induced drag, both depending on the lift squared. For the Nacra-17 rig, the effective span was predicted to be:

$$S_E = 0.719\ S_G \tag{8}$$

where S_G = 9.86 m is the distance from the mainsail headboard to the water surface of the flying catamaran. For simplification, this effective span was used to predict induced drag for the entire range of apparent wind angles.

The effective span of the Nacra-17 rig being 72% of the geometric span is significantly lower than the value for a typical ORC yacht. This may be due to the small jib, the foot of which does not reach any deck, but also due to the flying state of the catamaran, where the fly height adds to the geometric span, while the aerodynamic flow around the hull may add to the induced drag and thus reduce the effective span.

4.4 Sail Twist

Sail twist, the reduction of the angle of incidence of sail profiles with height, is commonly used by sailors to reduce the heeling moment of the aerodynamic forces. It is thus a second method to depower the sail, besides flattening or opening the sail with the traveler, the latter ones both being linear reductions of the sail's lift coefficient. While most VPPs account for linear lift reduction through a flattening factor, sail twist as an independent trimming parameter is rarely considered.
If twist is applied to reduce the heeling moment, two phenomena occur: the vertical center of the flow forces is lowered, which is the desired effect, and the induced drag is increased due to a less favorable lift distribution along the sail span.

An early study to introduce twist into a VPP has been presented by Jackson (2001), who predicts both the change of center of effort as well as effective span by integrating profile lift over span of the sails. While this approach models the physical properties of the sail correctly, it is hard to integrate into my VPP because of the computational costs. Fossati et al. (2006) modelled twist based on wind tunnel test results, obtained from the Politecnico di Milano wind tunnel. They use a twist parameter, derived from the ratio of the center of effort height and its optimum value. Due to measurement results influenced by flow separation phenomena, they abandoned using an independent twist parameter and combined flattening and twisting of the sail in a so called "power" parameter. The ORC measurement system, Offshore Racing Congress (2024), is based on a VPP and uses a twist factor, which depends on the flat factor. While this approach showed to be quite successful within the measurement system, it does not allow twisting and flattening the sail independently. For example, a trim with flat sails but very small twist, a common sail trim under flat water / constant wind conditions, cannot be modelled with this approach.

The method implemented in the Nacra-17 VPP uses a correction of the vertical center of effort and the induced drag, which is derived from vortex lattice grid calculations. This correction holds for the Nacra sail plan only and is not generalized. A generalization of this method is in the works.

The wind tunnel tests conducted for this project use a manual sail trim method: for each apparent wind angle, a sail trimmer trims the sails for maximum driving force, regardless of the heeling moment generated by the sails. Due to the flow separation at the top of an untwisted sail, trimming for maximum driving force usually involves some initial twisting of the sail.

If some additional twist is applied to reduce the heeling moment, a correction of the vertical center of effort and the induced drag is applied to the wind tunnel test results. For the sake of simplification, this is modeled with a linear correction of both the drag coefficient and the vertical center of effort:

$$c_D = c_{D\,wt} + \frac{\partial c_D}{\partial twist} twist \tag{9}$$

$$vce = vce_{wt} + \frac{\partial vce}{\partial twist} twist \tag{10}$$

where $c_{D\,wt}$ and vce_{wt} are the drag coefficient and the vertical center of effort from the wind tunnel tests, the latter one being normalized with the distance of the main headboard to the water surface. The linear change rates $\partial c_D / \partial twist$ and $\partial vce / \partial twist$ are computed with a lifting surface method, Graf (2014). Details of this investigation are subject to publication in preparation.

For the Nacra-17 rig, the following change rates of drag coefficient and vertical center of effort are used:

$\frac{\partial c_D}{\partial twist} = 8.62 \cdot 10^{-4}$ and $\frac{\partial vce}{\partial twist} = -2.42 \cdot 10^{-3}$

4.5 Sailing Forces under Sailing Conditions

Aerodynamic forces under true sailing conditions were calculated from the wind tunnel test results using an additional trim factor *flat*, considering the depowering of the sails by a linear reduction of the lift coefficient and the spanwise force coefficient. Sail twisting formulas are as follows:

$$c_{L\,sailed} = c_L \cdot flat \tag{11}$$

$$c_{D\,sailed} = c_D + CE\, c_L^2\, flat^2 + \frac{\partial c_D}{\partial twist} twist \tag{12}$$

$$c_{S\,sailed} = c_S \cdot flat \tag{13}$$

The moment coefficients are treated as if they are generated by lift only; thus, they are linearly reduced by *flat*, similar to (11).

Note that the *flat* factor represents any linear lift reduction, whether caused by sail flattening or by reducing the sail angle of incidence through traveler easing.

Lift, drag and spanwise force as well as the moments around the axes of the DLS-coordinate system are calculated from the coefficients, the reference sail area A_{Ref} and the apparent wind speed *AWS* using (3) to (5). *AWS* incorporates height-dependent true wind speed *TWS(z)*, true wind angle *TWA*, leeway angle *LW* and heel angle ϕ as to (14):

$$AWS(z) = \sqrt{\left(TWS(z)\cos TWA + U\cos(LW)\right)^2 + \ldots} \\ \overline{+\left(TWS(z)\sin TWA\cos\phi + U\sin(LW)\right)^2} \tag{14}$$

Since wind speed measurements in the wind tunnel are taken at the mast top, the true wind speed is also valid at this height in reality.

Forces and moments are transferred to the *x’,y’,z’* coordinate system. Here, the model accounts for the reduction in the centers of effort caused by sail twist.

$$M_{x'sailed} = M_{x'} + F_{y'} \frac{S_E\, \partial vce}{\partial twist} twist \tag{15}$$

$$M_{y'sailed} = M_{y'} + F_{x'} \frac{S_E\, \partial vce}{\partial twist} twist \tag{16}$$

where SE is the distance from the main headboard to the water surface at rest. The flat and twist factors accounting for the depowering of the sails are calculated within the VPP as decision (or free) variables in the optimization procedure.

5 RANSE FLOW SIMULATIONS

Flow forces generated by the daggerboards, the hull and the rudder are predicted using a proprietary OpenFOAM-based free-surface RANSE-solver. This solver has been described by Meyer et al. (2016), and a yacht-related investigation employing this solver has been presented at a previous InnovSail conference, Graf et al. (2017). The above publications include an intensive validation study for sailing yacht applications, albeit for appended monohulls only.

Compared to the standard OpenFOAM solver for free-surface flow, *interFoam*, our solver features some advanced algorithms for the treatment of the free surface: the high precision volume-of-fluid advection differencing scheme BRICS, a pressure reconstruction scheme at the free surface and non-reflective boundary condition at the inlet and outlet of the flow domain. As a result, the solver maintains a non-diffusive sharp air–water interface, suppressing numerical ventilation of submerged flow bodies and an increased computational efficiency, allowing quite large Courant-numbers.

6 DAGGERBOARD AND RUDDER FLOW FORCES

Daggerboard flow forces were investigated in the study reported in the predecessor of this publication, Graf and Freiheit (2020). The results achieved there were used here as well.

The Nacra-17 rudder design has changed since the Olympic games 2020(21). The rudder T-bar size has increased slightly and is now arranged asymmetrically. At the tips of the T-bar, the profiles are thickened. Most importantly, the rudder rake angle controlling the vertical forces generated by the rudder can now be changed during the races. This allows the crew to adapt the rudder rake to different wind speeds and courses, particularly to upwind and downwind courses. Before this new regulation was introduced, the rudder had to remain constant during a race, which made foiling more difficult.

Daggerboard and rudder flow forces were predicted from RANS-flow simulations using grids of approximately 2.6 million grid cells. The grids were generated using the split-cartesian approach with OpenFOAM's *snappyHexMesh* tool (Figure 8). The average normalized wall distance of the innermost cell is approximately y^+=50. Inlet boundary conditions are set to a given flow speed and turbulence intensity of 0.1% and a length scale of 2 mm, approximately the average boundary layer thickness. The simulation uses the k-ω-*SST* turbulence model; see Menter (1992).

Figure 9 shows the rudder-generated wave patterns at a velocity of U=9m/s at zero leeway and pitch.

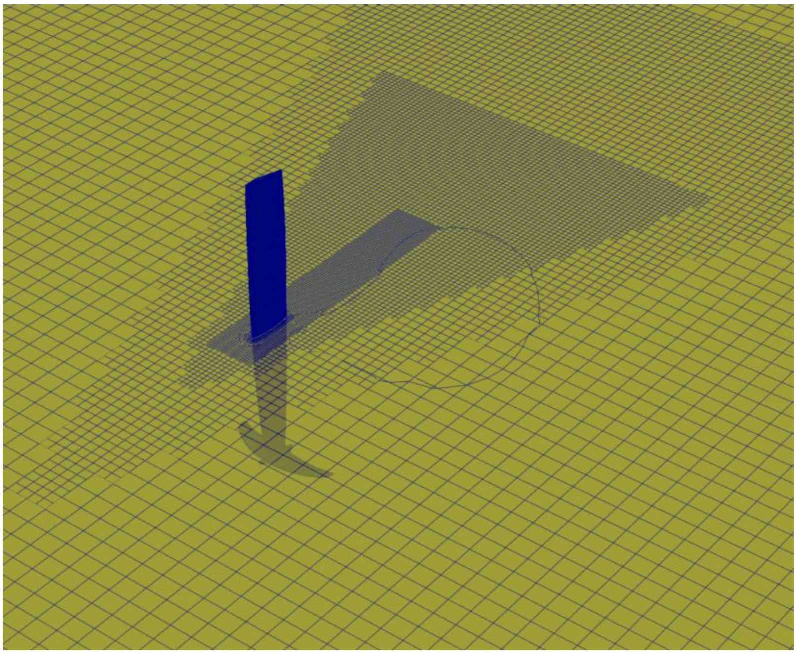

Figure 8. Split Cartesian Grid around Nacra-17 rudder

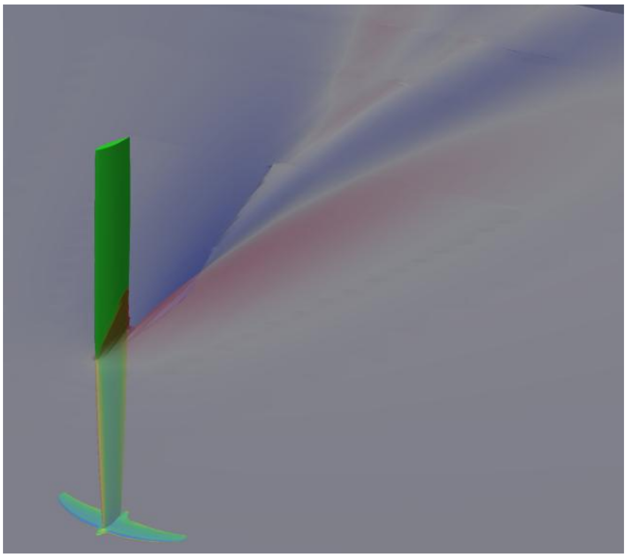

Figure 9. Nacra-17 rudder wave pattern at 9 m/s, zero leeway

A regression approach was used to calculate the flow forces within the VPP. Regression coefficients were derived from the RANS-investigation results.

CFD-predicted flow forces are converted into force areas by normalizing them with dynamic pressure. For lift *L,* the lift area *AL* is calculated as follows:

$$AL = \frac{L}{\frac{1}{2}\rho U^2} \tag{17}$$

with the density of water ρ and the flow speed *U.* Similar expressions are used for the drag force area *AD* and the spanwise force area *AS*. Force areas were approximated using the following regression formulas:

$$AL = \left(AL_0 + \frac{\partial AL}{\partial LW} LW + \frac{\partial AL}{\partial pitch} pitch \right) \cdot (1 - l_f \frac{fly}{1000mm})(U / 10m/s)^{l_u} \tag{18}$$

$$AS = \left(AS_0 + \frac{\partial AS}{\partial LW} LW + \frac{\partial AS}{\partial pitch} pitch \right) \cdot (1 - s_f \frac{fly}{1000mm})(U/10m/s)^{s_u} \quad (19)$$

$$AD = (AD_0 + \frac{\partial AD}{\partial LW} LW + \frac{\partial AD}{\partial Pitch} pitch + \frac{\partial^2 AD}{\partial LW^2} LW^2 + \frac{\partial^2 AD}{\partial pitch^2} pitch^2 + \frac{\partial^* AD}{\partial LW \, \partial pitch} LW \, pitch) \cdot (1 - d_f \frac{fly}{1000mm})(U/10m/s)^{d_u} \quad (20)$$

The coefficients $AL_0; \frac{\partial AL}{\partial LW}; \frac{\partial AL}{\partial pitch}; l_f; l_U$ and respective expressions for drag and spanwise force are derived from the simulation results using least-square-minimization. Figure 10 and Figure 11 demonstrate the accuracy of the fit for lift area *AL* and spanwise force areas *AS* (left) and drag area *AD* (right) for both daggerboard and rudder.

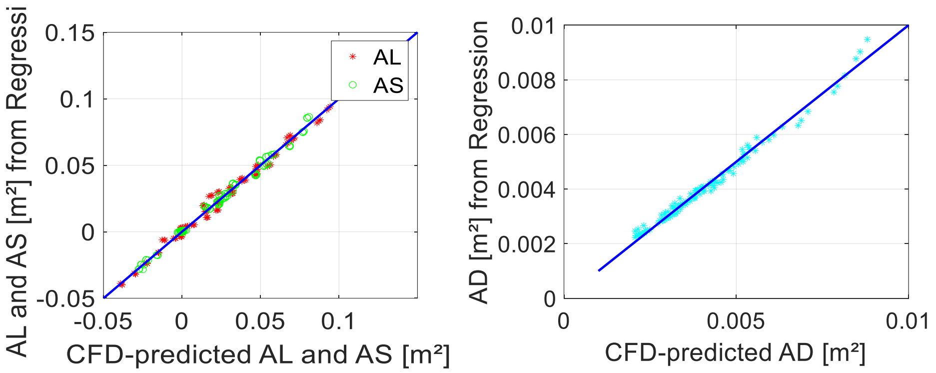

Figure 10. Fit of the daggerboard force regression against CFD results

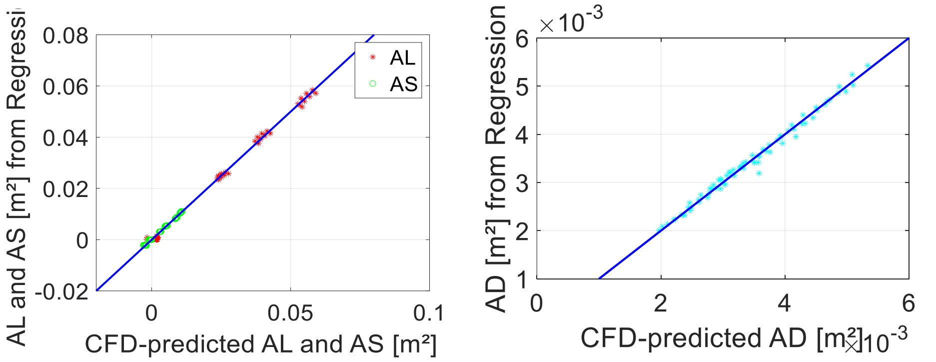

Figure 11. Fit of the rudder force regression against CFD results

7 HULL RESISTANCE

Resistance has been predicted for a single hull, neglecting wave reflection and interaction effects between hulls. In addition, the impact of trim and leeway on hull resistance has been neglected as well. Consequently, a test matrix with a permutation of boat speeds and buoyancies was investigated.

The computational grid was generated using the ANSA© meshing tool and uses dodecahedra cells in the far field of the flow domain, pentagon prisms to resolve the free surface, and prism layers around the hull for the boundary layer resolution (Figure 12). Approximately 2.5 million grid cells were used.

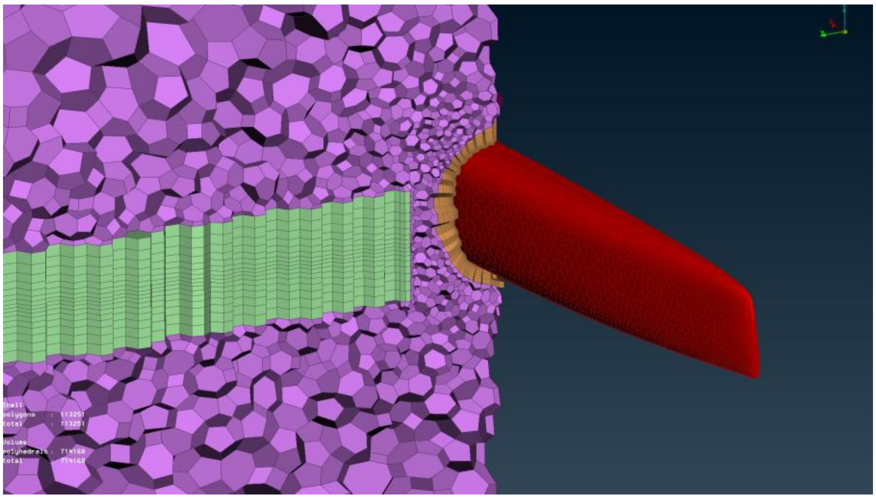

Figure 12. Polyhedral grid around Nacra 17 hull

The setup of the hull resistance investigation is similar to that used for the daggerboards. The hull was allowed to translate in a vertical direction and rotate around the transverse axis for fixed hydrostatic forces and moments. Investigated flow speed fully covers the upwind speed range and the downwind speed range to a quite high degree. The maximum investigated buoyancy conforms to the weight of the catamaran in sailing condition, mimicking the case of only one hull flying and no vertical foil forces. Flow speed and buoyancy were set as follows:

- Flow speed: U = 3 m/s; 6 m/s; 9 m/s
- Buoyancy: V = 0.1m³; 0.2 m³; 0.340 m³

The following contour plots show the wave pattern around the hull with a buoyancy of 0.34 m³ and for various flow speeds. At a hull speed of U = 3 m/s (Fn=0.42), a rather conventional wave pattern can be seen, while at U = 9 m/s, the wave pattern is very narrow, indicating the high Froude number of this hull speed. Some sprays also cover the deck zone of the hull at the highest speed.

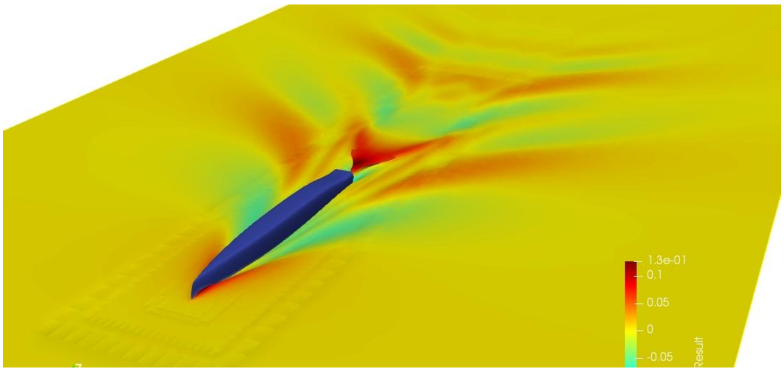

Figure 13. Wave pattern around the hull at u = 3 m/s

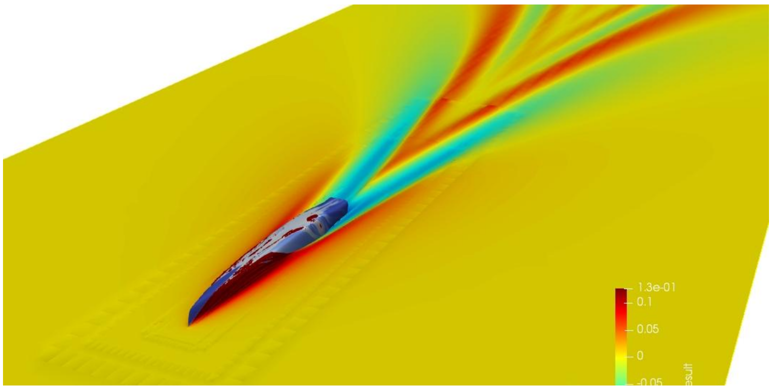

Figure 14. Wave pattern around the hull at u = 9 m/s

Figure 15 shows the resistance of a single float as a response surface for cubic spline interpolation within the VPP.

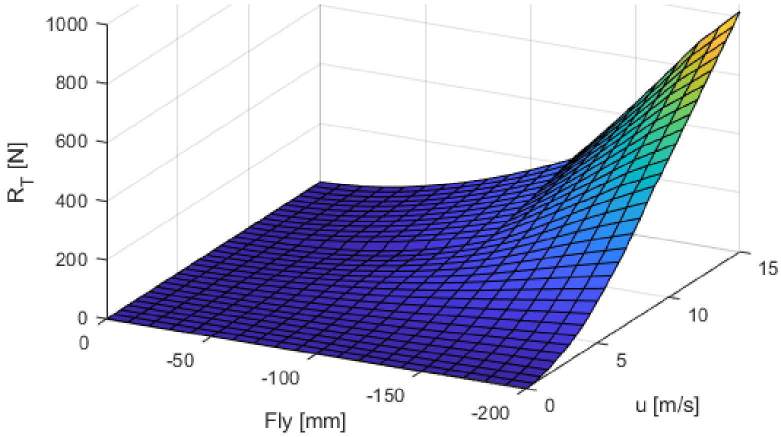

Figure 15. Nacra-17 resistance diagram. The fly height of the hull is zero if it just touches the free surface at rest.

Some towing tests with the hull and rudder were made in full scale and used for validation. Field tests generally lack some accuracy compared to tank tests, since the impact of environmental changes can never be entirely excluded. During the resistance tests, a light breeze prevailed. To minimize its impact on the measured resistance, two towing tests were conducted: one attempt with headwind and another with wind from astern. These tests were conducted without daggerboards, but rudders were necessary to keep the boat on track. Figure 16 shows the results of the towing tests compared to the computational resistance results. In this case, the calculated resistance consists of CFD results for the hulls and some empirical formulas for the rudder resistance. The windage of the platform with crew on board was derived from a tare wind tunnel measurement.

Given the expected inaccuracy of the field test results, the agreement of the field test with computed resistance seems to be acceptable.

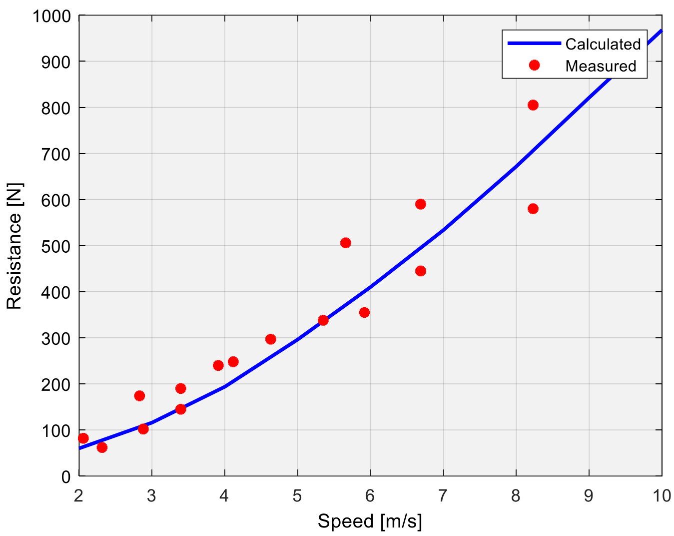

Figure 16. Towing test results and comparison with numerical prediction

8 VELOCITY PREDICTION

Constrained optimization methods were used to predict Nacra-17 velocity. Boat speed was calculated using:

$$\min_{\mathbf{x}} f(\mathbf{x}) \tag{21}$$

subject to the equality constraints:

$$\mathbf{G} = \begin{Bmatrix} \sum F_X \\ \sum F_Y \\ \sum F_Z + m_T g \\ \sum M_Y \\ \sum M_Z \end{Bmatrix} = 0 \tag{22}$$

and inequality constraint:

$$\mathbf{H} = \left\{ \sum M_X - M_{R\max} \right\} \leq 0 \tag{23}$$

where f is the objective function, set to $f = -U\cos(LW)$ for maximization of boat speed and $f = -U \cdot \cos(TWA + LW)$ for *VMG* maximization. The equality constraint $\mathbf{G} = 0$ says, the aerodynamic and hydrodynamic forces in X, Y and Z-direction and moments around the Y- and Z-axis are in equilibrium. The inequality constraint $\mathbf{H} \leq 0$ says, that the sum of aerodynamic and hydrodynamic heeling moments is smaller or equal to the maximum righting moment M_{Rmax}. With the total center of gravity assumed to be 0.8 m above the water surface, the maximum righting moment occurs at a windward heeling angle.

The total mass m_T is the sum of the light ship weight, 134 kg according to class regulations, plus a crew weight in the same order of magnitude. The maximum righting moment was calculated with a crew arm of 2 m. The static moment around the Y-axis is calculated with a center of gravity of the light ship weight 0.4 forward of the origin and the crew weight times the longitudinal crew arm l_{Crew}, the latter one being a free variable.

$\mathbf{x}$ is the vector of free variables:

$$\mathbf{x} = \left\{ pitch_L, pitch_W, pitch_P, pitch_{RL}, pitch_{RW}, heel, flat, twist, fly, RA, U, LW, heel, l_{Crew} \right\}^T \tag{24}$$

where $pitch_{L,W,RL,RW,P}$ are the pitch angles of the leeward and windward daggerboard and rudder and the entire platform. *flat* and *twist* are the flattening and twisting of the sails. The state variables of the catamaran are boat speed U, leeway angle LW, heeling angle $heel$, fly height fly and rudder angle RA. In the context of constrained optimization, the state variables are free variables subject to optimization, since they are set to values to establish fulfilment of the constraints.

A variation of the model neglects moment equilibrium about the upright axis, assuming sufficient mast rake to achieve yaw-moment balance at the optimal rudder angle. This aspect is critical for a semi-L foil, where side-force distribution between the daggerboard and rudder strongly affects foiling onset; in light wind conditions, the daggerboard must carry nearly 100% of the side force to enable early take-off. This normally results in low rudder angles and a potentially lee helm. Discussions with sailors indicated a dislike for this trim, as some degree of windwardness is required for effective upwind steering; accordingly, the model sets the lower bound of the rudder angle to 0°.

Besides the nonlinear equilibrium and inequality constraints, bounds were given for all free variables. These are set to reasonable values derived from mechanical limits due to class rules and the construction of the hull and daggerboard. Some of the bounds (e.g., heel) are assumed from general sailor consensus.

The VPP is implemented using the *Matlab©* computational environment. For constrained optimization, the *interior point* method is used in a black box style. No effort was made to enhance or improve the methods readily available in *Matlab*. A multistart strategy was employed to identify the best solution over the design space. Initial candidates were drawn from a Sobol sequence to ensure space-filling coverage, and a constrained interior-point optimization was applied for each starting point. This approach is likely to locate the global optimum.

9 OPTAINING OPTIMAL DAGGERBOARD AND RUDDER SETTINGS FROM VPP RESULTS

The results presented here focus on upwind sailing. Some downwind VPP results are shown in the authors' previous publication. The rationale behind this has been given by the sailors, who were more interested in upwind optimization, in particular upwind foiling onset in light wind conditions.

9.1 Upwind Velocity Polar

Figure 17 shows the velocity polar, the diagram depicting boat speed as a function of a true wind angle 30° ≤ *TWA* ≤ 90°, and a true wind speed 5kts ≤ *TWS* ≤ 19kts. Generally, the diagram shows that boat speeds higher than two times wind speed can be achieved for lower wind speeds, and in strong wind conditions, the boat speed achieves 1.5 times wind speed. As expected, these high boat speeds occur on the beam reach.

A few additional observations can be made:

- For *TWS* ≤ 7 kts, no transition to the flight state can be seen.
- For higher wind speed, the transition to flight condition can be identified by a discontinuity in the slope of the graph. For TWS = 8 kts, the catamaran is mainly non-flying with some flying states at TWA=75° and TWA=90°. The change from flying to non-flying state at this wind speed is not completely plausible and so the results cannot really be trusted here.

The velocity polar for *TWS* = 9 kts and TWS = 10 kts are of particular interest. Here, two local maxima of *VMG* can be seen: at *TWA*≈45° at a non-flying state and a slightly higher *VMG* at TWA≈55° at a flying state. At these wind speeds, the crew actually has two options on an upwind tack: sailing at smaller true wind angle non-foiling, but with tactically safe sailing. For the second option, the crew has to bear away slightly to true wind angles of TWA≈ 60° and the boat would enter a foiling state with significant speed gains.

Discussions with the sailors resulted in a valuation that the second option is quite risky and will only be chosen in a tactically clear situation, where foiling is successful for the whole leg and will not be interrupted by possible right-of-way situations. However, this choice can strongly influence race outcomes.

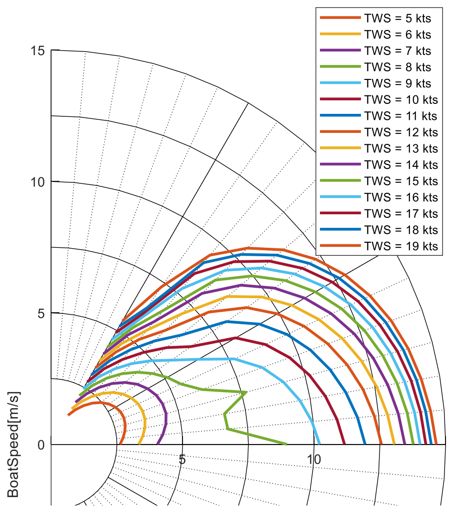

Figure 17. Nacra-17 upwind velocity polar

9.2 Max VMG Upwind

Nacra-17 races are usually up-and-down-races. Consequently, optimization of *VMG* is more interesting to sailors than speed optimization for a given true wind angle. For *VMG* maximization, the objective function *f* for optimization is not the negative speed of the catamaran, but rather:

$$f = -U \cdot \cos(TWA + LW) \tag{25}$$

In this particular case, the true wind angle is an additional free variable subject to optimization.

Figure 18 shows achievable boat speed as well as optimized values for true wind angle *TWA* and fly height over true wind speed *TWS*. We can see that Nacra-17 can fly on an upwind course as soon as the true wind speed exceeds 9 kts. This number is confirmed by sailors: some claim that flying can even start at slightly lower wind speeds.

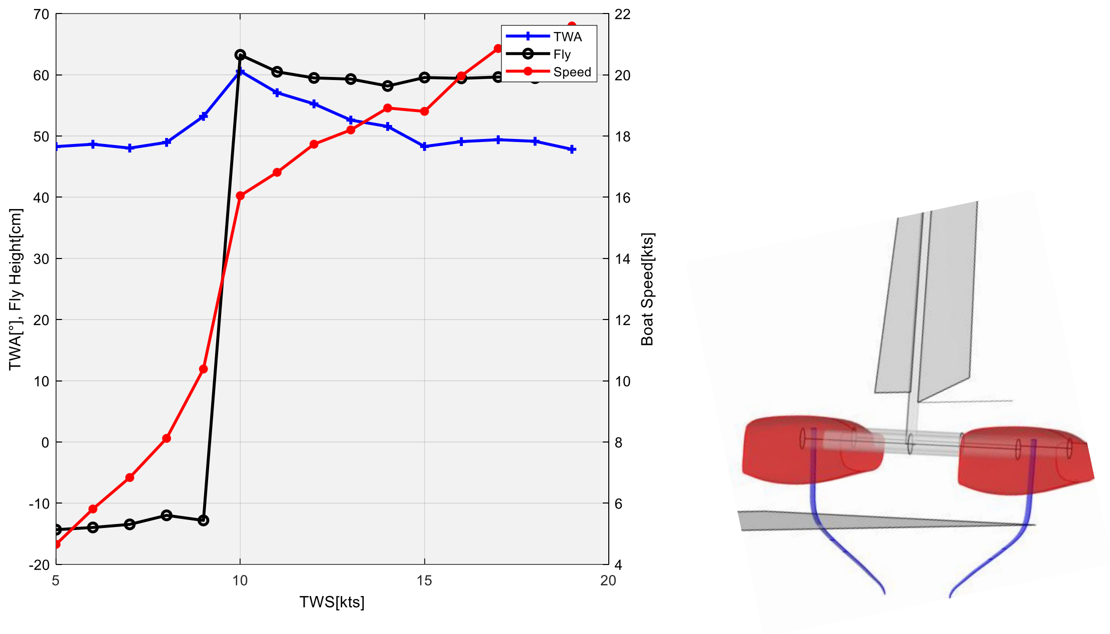

Figure 18. Nacra-17 speed, fly-height and *TWA* as a function of *TWS*, **right image depicting fly height of 600 mm**

For *TWS*<9kts, the boat does not fly (*fly*<0). At higher TWS, the fly height changes quite rapidly, and the boat seems to jump to a stable flying state. Practical observations show that flight stability decreases when the daggerboard knee emerges from the water; sailors therefore avoid this condition by applying an appropriate longitudinal trim.

From an optimal true wind angle of about TWA≈45° at a non-flying state, the sailors have to bear away with increasing wind speed in order to get an early flying state. To get to a flying state at TWS=9kts, the TWA angle has to be as large as TWA=60°. With wind speeds continuing to rise, the true wind angle can be reduced again. This pattern fits well with the sailors' descriptions of the respective situation.

Some effort was made to validate these results. During races, onboard measurement devices—particularly GPS—provide position tracking and speed-over-ground data. However, no wind measurement instruments are on board. The data shown in Figure 19 are obtained with the help of a coach boat, equipped with an anemometer for wind speed. The sailors on board are assumed to sail an apparent wind angle for maximum VMG; however, in the training situation, they are not always trying to maximize boat speed. Consequently, the measured speed values are very noisy, making any comparison of field data with computed data very difficult. Because a VPP always predicts the maximum achievable speed while measurements reflect degraded real-world performance, the VPP-predicted speed progression can be regarded as an upper-envelope curve of the measured data. Two findings can be drawn:

- For true wind speed TWS<11kts, the computed boat speed agrees acceptable well with the maximum boat speeds measured.
- Beyond TWS≥11kts, the computed boat speed still increases while the maximum measured boat speeds remain approximately constant.

Discussions with sailors indicated that, at higher wind speeds, maintaining stable sailing conditions becomes increasingly more important than continuously pursuing maximum boat speed, which can degrade performance.

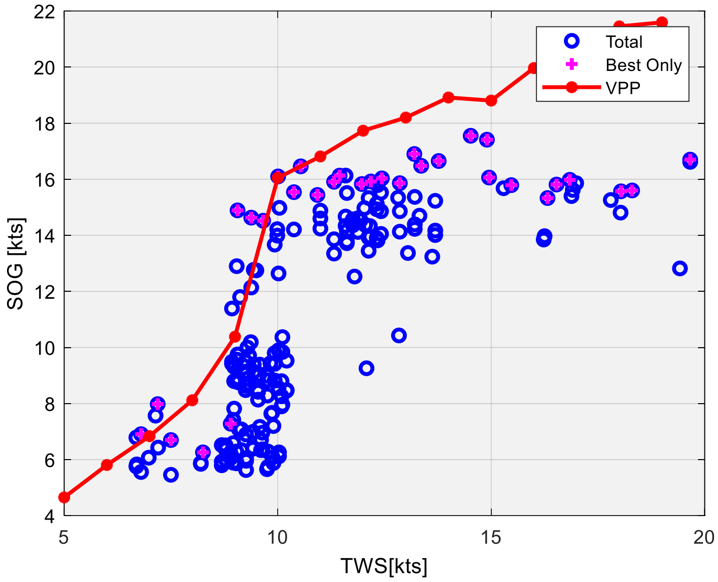

Figure 19. VPP results vs. field measurements

9.3 Daggerboard and Rudder Settings at Optimum VMG Courses

The following diagrams show the daggerboard and rudder settings for achieving maximum VMG. Figure 20 can be seen as a sailing instruction for the daggerboards and the rudders. It shows the pitch angles of the two daggerboards and the two rudders over the true wind speed TWS.

Figure 20 indicates that in non-flying states, the rudder pitch should be identical on both windward and leeward tacks. The rudder pitch is low in order to reduce resistance and to load the daggerboard with side force to allow early flying. With increasing wind and as soon as flying is possible, the rudder pitches should be set independently. The leeward rudder produces vertical lift with pitch angles between 2° and 4°, while the windward rudder should be set to a lower pitch angle which here is limited by 0°. This difference of the rudder pitches is known as 'rudder differential' by the sailors and contributes to the righting moment. Note that the possible range of rudder pitch is limited to 4° by class regulations. Here, a range of $0° \leq pitch_{Rudder} \leq 4°$ is used. A range of $-0.5° \leq pitch_{Rudder} \leq 3.5°$ has also been tested but resulted in less favorable flying onset.

The daggerboard pitches were quite low under light-wind conditions. At a very light wind, the VPP finds optimum settings for the daggerboard, where the windward foil is pitched higher than the leeward foil, a result not being really intuitive. However, if flying is not possible due to light wind, the optimizer tries to minimize resistance by keeping the vertical lift and accompanying induced drag low. The windward foil is assumed to generate less drag for a given side force and neglected vertical force.

With increasing wind speed, the pitch of the leeward daggerboard increases to a maximum of 6° as soon as the boat foils. The windward daggerboard pitch decreases and is even getting negative at wind speeds above 12 kts. Again, the difference in foil pitches contributes to the righting moment.

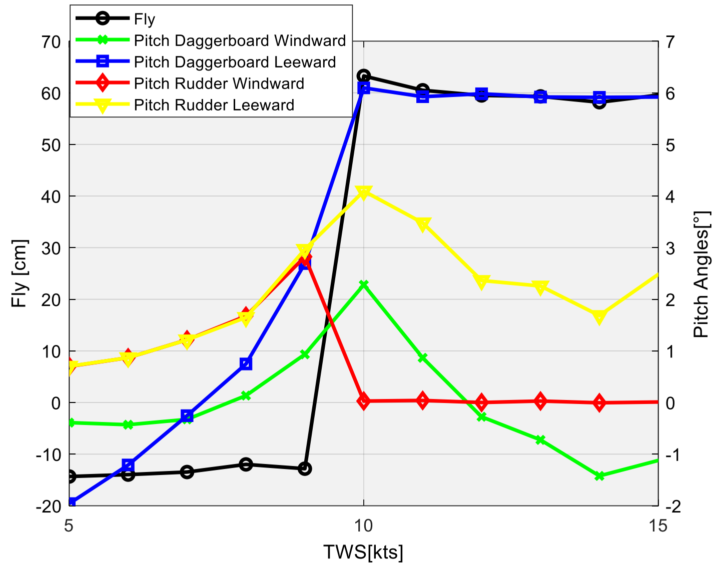

Figure 20. Pitch (rake) angles of daggerboards and rudders

Figure 21 shows the optimized rudder and heel angle over true wind speed. It depicts that the transition to a flying state is supported by a small leeward heeling angle when the boat is in transition from non-flying to flying state. This is due to the shape of the semi-L daggerboard. A leeward heel angle increases the vertical component of the lift of the lower part of the daggerboard. As soon as the boat is flying, the optimum heel angle drops to values around 0°. At higher wind speeds, the optimum heel angle is even negative. Since the vertical center of gravity is well above the water surface, any windward heel contributes to the righting moment. This result is quite well known from catamarans with true L-shaped daggerboards, where the windward foil is taken out of the water, see Figure 22 for clarification.

These findings were discussed with the sailors, who stated that, in sailing practice, this variation in heeling angle is difficult to realize. In non-flying condition leeward heels normally slow the boat, so sailors must be confident that inducing leeward heel will lead to a flying state, yielding the advantage bound to it. Windward heel in strong wind conditions is also unpopular among Nacra-17 sailors, as maintaining this state over a longer period on the upwind leg is difficult.

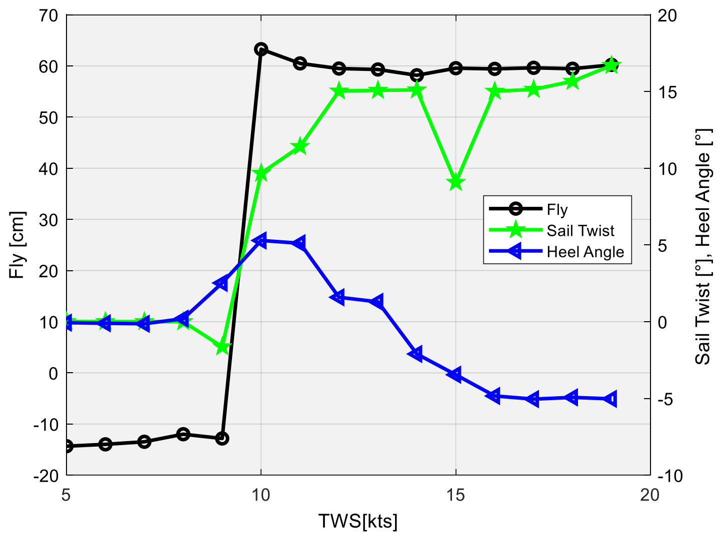

Figure 21. Nacra-17 optimized heel angles and sail twist

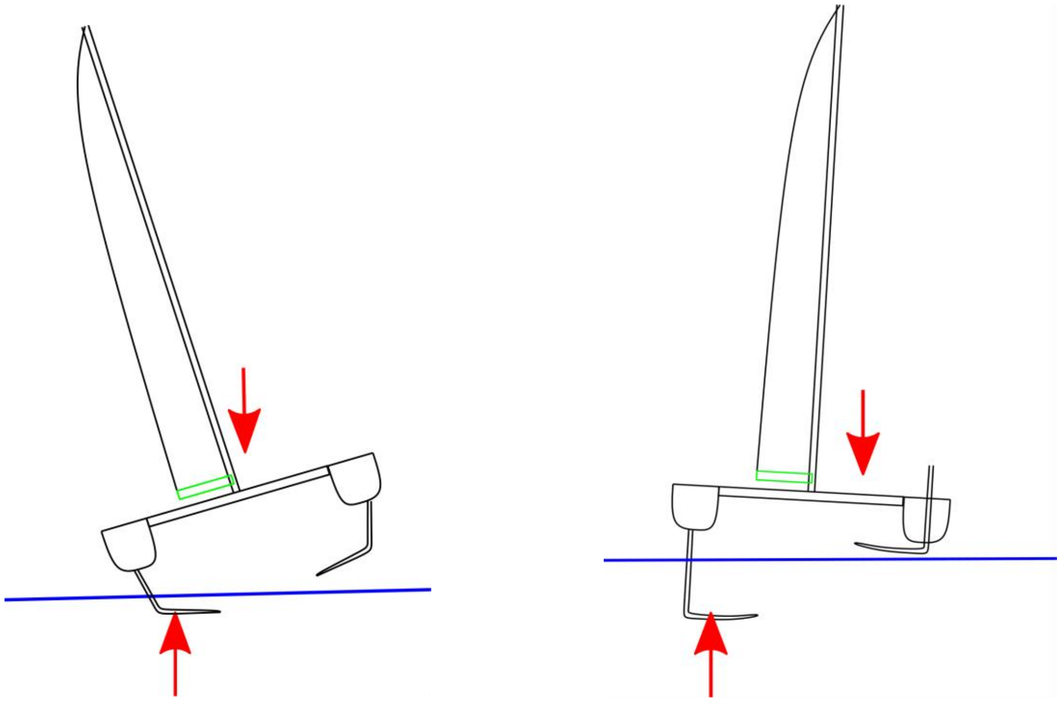

Figure 22. Daggerboard forces and righting moment at windward and leeward heel. Leeward heel increases production of the vertical component of daggerboard lift, allowing early flying in light wind conditions. Windward heel increases the righting arm due to high VCG, increasing performance in strong wind conditions.

Figure 21 also shows the twist of the main sail. As expected, the twist is low as long as the wind speed is low, but as soon as the wind speed is strong enough to reach righting moment limitations and is sufficient for the boat to fly, a twist angle of approximately 15° is found to be optimal. Finding an optimum twist is quite hard for a numerical optimizer because the impact of twist on the performance is rather low compared to other state variables like leeway and boat speed, making the solver prone to instabilities, as can be seen for the results at TWS=15kts.

9.4 Impact of Crew Weight on Performance

In the late preparation period for the Olympic sailing games in Marseilles 2024, the question arose about what impact crew weight has on boat performance. In contemporary sailing, small changes in crew weight are commonly understood to be free variables within an optimization loop. The expectations are quite clear: lower crew weight increases performance in light wind conditions due to the lower resistance of hull and foils, while higher crew weight increases performance in strong wind conditions where the maximum righting moment usually is a strong performance driver.

To identify quantitative measures and crossover points, the performance obtained in Chapter 9.3 is compared with performance under identical conditions but with the crew weight reduced by 10 kg. Figure 23 shows the outcome of this study.

At non-foiling states and wind speeds below TWS = 9kts, a lower crew weight results in significantly better boat speed. The crossover point, where additional crew weight starts to increase performance, is at TWS=9kts. A higher crew weight enables an earlier transition to a flying state, and increasing wind speed further amplifies the performance advantage of a higher crew weight.

In light of the expected light wind conditions in Marseilles, the range of wind speeds $5kts \leq TWS \leq 9kts$ was examined more closely. Figure 23 right shows that the lighter crew will reach the windward mark of a 1 nm upwind tack between 6 and 10 seconds earlier, leaving the heavier boat 15 to 25 meters behind.

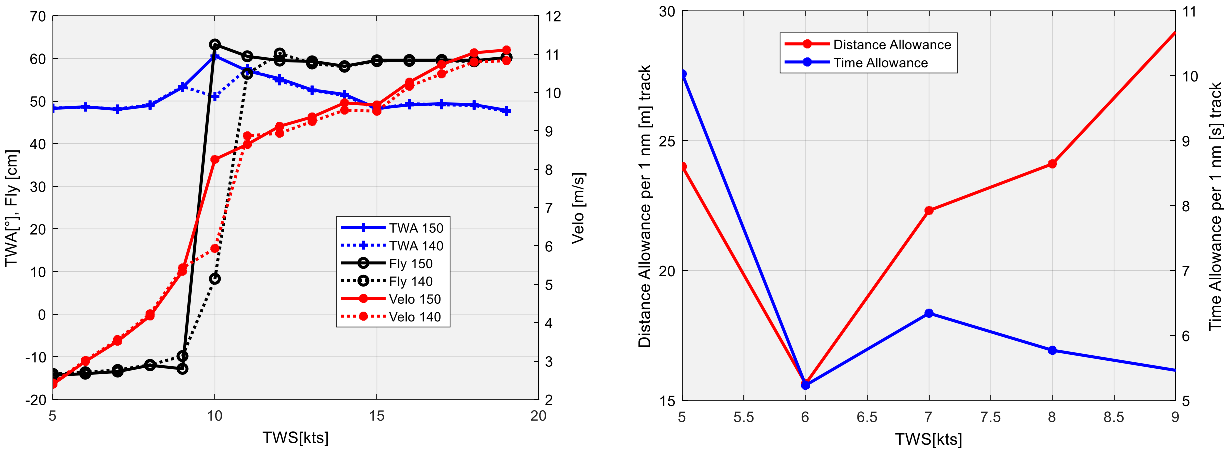

Figure 23. left: Performance comparison for crew weight of 150 kg and 140 kg, right: time and distance allowances for a reduction of crew weight by 10 kg

10 CONCLUSIONS

This project aimed to develop a method that assists Nacra-17 Olympic catamaran sailors in maximizing boat performance. This was solved by means of a VPP, which calculates the maximum achievable boat speed from a force-and-moment equilibrium with a set of optimized boat trim parameters. The VPP is able to quantify many optimum trim settings, such as daggerboard and rudder rake, which so far have been optimized by sailors through practical sailing or reasoned conclusion.

During the course of the study, numerous meetings were held with the sailors, discussing the theoretical findings and comparing them with practical experience. This always led to the theoretical side being enriched by the sailors and the sailors receiving inspiration from theory. Generally, both sides gained from cooperation and theory and praxis converged over the course of the study.

Various limitations and shortcomings of the existing procedure should be addressed in future studies.

- Ventilation and cavitation: While ventilation of the foils in the vicinity of the free surface is considered by the free-surface calculation method, this is rather rudimentary and neglects transient effects the sailors often report about. Cavitation was not considered at all.
- Daggerboard flexibility significantly affects performance but is represented only by a small increment in the effective heeling angle experienced by the daggerboards; this rudimentary treatment requires further refinement.
- The forces generated by the daggerboards are calculated assuming a fully turbulent flow. With a Reynolds number in the regime of laminar-turbulent transition, this assumption degenerates the results. Also, the surface roughness of the daggerboard and rudders is a topic of constant discussion by sailors, while it is completely neglected by theoretical studies. Given the current availability of reliable methods for predicting laminar–turbulent transition, this deficiency can be remedied easily.
- Finally, the hull resistance model neglects trim and leeway effects, and the test matrix remains limited; with sufficient computational power, this deficiency can be eliminated straightforwardly.

ACKNOWLEDGMENTS

The author would like to thank the sailors of Team Kohlhoff-Stuhlemmer for their excellent cooperation. I would also like to thank the German Sailing Association, in particular the technical coach, for its support, provision of technical data, and practical contributions.

REFERENCES

Clauthon, A., Wellicome, J. and Shenoi, A. (1998). Sailing Yacht Design, Theory. Addison Wesley Longman Limited, Essex/GB.

Hazen, G.S. (1980). A Model of Sail Aerodynamics for Diverse Rig Types. Proc. New England Yacht Symposium. New London, Connecticut/USA.

Offshore Racing Congress (2024). ORC VPP Documentation 2024 https://orc.org/for-designers/orc-vpp.

Meyer, J., Renzsch, H., Graf, K. and Slawig, T. (2016). Advanced CFD-Simulations of free-surface flows around modern sailing yachts using a newly developed OpenFOAM solver. Society of Naval and Marine Engineers (Ed.): The Twenty-Second Chesapeake Sailing Yacht Symposium, Annapolis/USA.

Fossati, F., Muggiasca, S. and Viola, I. (2006). An investigation of aerodynamic force modelling for IMS rule using wind tunnel techniques. 19th HISWA Symposium on Yacht Design and Yacht Construction, Amsterdam/NL.

Graf, K., Meyer, J., Renzsch, H. and Preuss, C. (2017). Investigation of modern sailing yachts using a new free-surface RANSE code. Cite de la Voile Eric Tabarly and Naval Academy Research Institute (Ed.): Innovation in high performance sailing yachts (InnovSail 2017), Lorient/FR.

Jackson, P.S. (2001). An Improved Upwind Sail Model for VPP's. 15th Chesapeake Sailing Yacht Symposium, Annapolis/USA.

Nocedal, J. and Wright, S. (2016). Numerical Optimization, p 563ff. Springer Science + Business Media LLC.

Graf, K. and Freiheit, O. (2020). VPP-driven sail and foil trim optimization for the Olympic Nacra-17 foiling catamaran. Proc. 5th InnovSail, Ecole Naval de France / Brest.

Menter, F. (1992). Improved Two-Equation k-omega Turbulence Models for Aerodynamic Flows. NASA Technical Memorandum 103975.

Knudsen, S., Walther, B. and Marimon Giovannetti, L. (2023). Modelling Upwind Aerodynamics of the NACRA-17 with Dynamic FSI. Proc. 6th InnovSail. Ecole Navale de France / Brest.

Wackers, J., Koren, B., Raven, H.C., van der Ploeg, A., Starke, A.R., Deng, G.D., Queutey, P., Visonneau, M., Hino, T. and Ohashi, K. (2011). Free-surface viscous flow solution methods for ship hydrodynamics. Arch Comput Methods Eng 18: 1–41. DOI 10.1007/s11831-011-9059-4.

Graf, K. (2014). The Vortex Lattice Grid Method for the Calculation of Flow around Wings of Arbitrary Shape and Infinite Thin Thickness. Course script, University Applied Sciences Kiel, GER.